RSC Advances

PAPER

View Article Online
View Journal | View Issue

Cite this: *RSC Adv.*, 2022, **12**, 6592

Cytotoxic and photocatalytic studies of hexagonal boron nitride nanotubes: a potential candidate for wastewater and air treatment

Awais Khalid,[a] Pervaiz Ahmad,*[b] Abdulhameed Khan,[c] Mayeen Uddin Khandaker,[d] Imen Kebaili,[ef] Md Mottahir Alam,[g] Israf Ud Din,[h] Saleh Muhammad,[a] Zohaib Razzaq,[a] Ibad Ur Rehman,[a] Habib Ahmad Abbasi[b] and Danish Hayat[i]

Received 15th January 2022
Accepted 16th February 2022

DOI: 10.1039/d2ra00300g

rsc.li/rsc-advances

Boron nitride (BN) nanomaterials are rapidly being investigated for potential applications in biomedical sciences due to their exceptional physico-chemical characteristics. However, their safe use demands a thorough understanding of their possible environmental and toxicological effects. The cytotoxicity of boron nitride nanotubes (BNNTs) was explored to see if they could be used in living cell imaging. It was observed that the cytotoxicity of BNNTs is higher in cancer cells (65 and 80%) than in normal cell lines (40 and 60%) for 24 h and 48 h respectively. The influence of multiple experimental parameters such as pH, time, amount of catalyst, and initial dye concentration on percentage degradation efficiency was also examined for both catalyst and dye. The degradation effectiveness decreases (92 to 25%) as the original concentration of dye increases (5–50 ppm) due to a decrease in the availability of adsorption sites. Similarly, the degradation efficiency improves up to 90% as the concentration of catalyst increases (0.01–0.05 g) due to an increase in the adsorption sites. The influence of pH was also investigated, the highest degradation efficiency for MO dye was observed at pH 4. Our results show that lower concentrations of BNNTs can be employed in biomedical applications. Dye degradation properties of BNNTs suggest that it can be a potential candidate as a wastewater and air treatment material.

1 Introduction

In recent years, one of the most important and vital study topics in biomedical sciences has been determining the pharmacological properties of nanomaterials.[1] Water is the most essential naturally occurring element, as it is essential for the existence of all living things, as well as food production and economic development. Water scarcity is currently affecting a vast number of nations around the world. According to estimates, almost 40% of the global food supply is manufactured through industrial processing that ultimately relies on water. Water quality and seasonal availability have a direct impact on economic success, social development, and environmental protection.[2,3] Water purity and quality are usually influenced by population growth, urbanization, industrialization, and other anthropogenic factors. The availability of pure water is influenced by global population growth, with billions of people facing a freshwater shortage.[4,5] Dyes are frequently used to decorate objects and contain various organic compounds.[6] They will do a lot of damage to water if they get into it.[7] Adsorption and photodegradation are the most frequent dye removal procedures.[8,9] According to research, millions of dyes including methyl blue (MB), methyl red (MR), methyl orange (MO), congo red, and Martius yellow, are used in many industries, including construction, leather, printing, metal processing, and paper.[10,11]

[a]*Department of Physics, Hazara University Mansehra, 21300 Khyber Pakhtunkhwa, Pakistan. E-mail: awais.phy@hu.edu.pk; saleh@hu.edu.pk; ibad.phy@hu.edu.pk; zohaib.phy@hu.edu.pk*

[b]*Department of Physics, University of Azad Jammu, and Kashmir, 13100 Muzaffarabad, Pakistan. E-mail: pervaiz_pas@yahoo.com; Pervaiz.pas@gmail.com; habibahmadabbasi333@gmail.com*

[c]*Department of Biotechnology, University of Azad Jammu and Kashmir, Muzaffarabad, Pakistan. E-mail: abdulhameed.khattak81@gmail.com*

[d]*Center for Applied Physics and Radiation Technologies, School of Engineering and Technology, Sunway University, Bandar Sunway, 47500 Selangor, Malaysia. E-mail: mayeenk@sunway.edu.my*

[e]*Department of Physics, Faculty of Science, King Khalid University, P.O. Box 9004, Abha, Saudi Arabia*

[f]*Laboratoire de Physique Appliquée, Groupe des Matériaux Luminescents, Université de Sfax, Faculté des Sciences de Sfax, BP 1171, 3000 Sfax, Tunisia. E-mail: imen_kbb@yahoo.fr*

[g]*Department of Electrical and Computer Engineering, Faculty of Engineering, King Abdul Aziz University, Jeddah 21589, Saudi Arabia. E-mail: mohammad.mottahir@gmail.com*

[h]*Department of Chemistry, College of Science and Humanities, Prince Sattam Bin Abdulaziz University, P. O. Box 173, Al-Kharj 11942, Saudi Arabia. E-mail: i.din@psau.edu.sa*

[i]*Department of Botany, Hazara University Mansehra, 21300 Khyber Pakhtunkhwa, Pakistan. E-mail: danishhayat000@gmail.com*

Water can be purified by using basic techniques to remove small impurities and salts, however removing toxic dyes and harmful metal ions with traditional experimental approaches is extremely difficult.[12,13] Water purification engineers and experts are increasingly questioning the current exercise's practicality in meeting the high water needs for customers while adhering to increasingly strict requirements.[14,15] Photocatalysis is a method of degrading contaminants by using photocatalysts and light irradiation. It is frequently applied in environmental remediation and energy production.[16,17] Because of the wide-band gaps of some photocatalytic materials, they can only destroy contaminants when exposed to ultraviolet light (UV).[18] It has been reported that under visible light irradiation, some materials including dyes can sensitize the photocatalyst with a wide bandgap. They transfer their electrons (photo-excited) into the conductive band, allowing the photocatalyst to degrade pollutants.

Boron nitride (BN) is a semiconductor with a wide (direct) bandgap of 5.97 eV.[19] BN in its stationary phase is stable at standard ambient temperature and pressure (SATP).[20] It has a structure similar to graphite, but instead of carbon atoms, it has boron and nitrogen atoms.[21]

Researchers have been paying close attention to BN-based nanomaterials in recent years due to their outstanding biocompatibility,[22–25] robust mechanical and chemical stability,[26,27] for their prospective uses in clinical applications. Due to its potential cellular internalization, scientists are trying to investigate its therapeutic efficacy for gene carriers and drugs delivery.[28,29] Nanostructures (NS) of h-BN have extraordinary physiochemical properties. Its nanosheets (BNNSs) are like that of graphene with alternative boron and nitrogen atoms, instead of carbon.[30] In addition to its similar mechanical properties and thermal conductivity to graphene,[31–34] BNNSs have many advantages over carbon. These features comprised a consistent bandgap (5–6 eV), thermal stability, oxidation resistance, and enhanced chemical inertness among others.[35,36] Because of these properties, BNNSs appears as a very efficient and enticing product for a range of applications. Devices made of BNNSs will be able to operate easily in high-temperature and oxidative environments. It can also be utilized to make insulating materials with exceptional mechanical and thermal properties.[31,37] Boron nitride nanotubes (BNNTs) are the rolled-up sheets of h-BN with all the excellent properties of other h-BN nanostructures. Due to the absence of a well-known synthesis technique, the characteristics and applications of BNNTs have continued to remain unexplored.

BNNTs are negatively charged, as a result, they are an excellent h + carrier acceptor and could therefore be used in photocatalysis to increase h^+/e carrier separation.[38] Combining BNNTs with photocatalysts can significantly improve photocatalytic activities by enhancing visible light absorption and lowering the hole/electron carrier recombination rates. As a result, the BNNTs could be a new photocatalyst with improved visible light-responsive photocatalytic activity.[39–41] Similarly, BNNTs and other nanostructures of h-BN have potential applications in the effective degradation of methylene blue from wastewater.[42] It has been found that nanonets of ultrathin fibrous BN have a great potential to clean water *via* ultrafast MB dye degradation.[43] However, the experiments to confirm the broad applicability of BN nanostructures are still in the process. Studies exist in which the main focus was on the efficient H_2 gas degradation on the surface of modified BN nanostructures.[44] BNNTs coated with Fe_3O_4 NPs have successfully been used for the removal of arsenic from water by effective adsorption on its surface.[45] BN is a chemically stable material that is frequently used to remove contaminants from water.[46] BN nanosheets (NSs) have excellent Cu(II) adsorption characteristics,[47] with an adsorption capacity of 678.7 mg g^{-1}.[48] Methylene blue,[49] tetracycline,[50] and rhodamine B[51] have adsorption capacities of 392.2 mg g^{-1}, 305 mg g^{-1}, and 210 mg g^{-1}. BN is an excellent material for water purification and has a wide range of applications.[52]

In the current work, the wide bandgap BNNTs are chosen to further explore their properties as a photocatalyst due to their widespread application in wastewater treatment. In addition, the current study is aimed to explore the cytotoxicity, and dye degradation properties of BNNTs. By using the experiential interpretation, this study also gives a thorough insight into the efficacy of BNNTs against cancer cells and as an improved dye degradation material for the effective removal of organic contaminants from wastewater. The impact of several parameters such as initial dye concentration, time, pH, and amount of catalyst on the performance of the produced BNNTs in the adsorption of methyl orange (MO) dyes has been investigated in detail.

2 Experimental details

2.1. Material and methods

The experimental set-up or system's main component in the current work consists of a typical horizontal quartz tube furnace. The set-up is set to run or heat (at 10 °C min^{-1}) and maintained a temperature of 1200 °C (for 2 hours). In an alumina boat, 50 mg crystalline boron-10 (^{10}B) powder is mixed with 25 mg MgO powder. After that, 25 mg of maghemite (γ-Fe_2O_3) powder (99.9% pure) is also added to the precursors and properly mixed.[53] A small one-end closed quartz tube is placed under the heating filament of the furnace in such a way that the closed-end was toward the gas inlet. The boat containing the precursors is carefully inserted towards the closed end in the tube. The furnace is switched on and the precursors are heated up to 1200 °C in the argon atmosphere (at a rate of 200 sccm). During this stage, the argon is replaced by ammonia gas and maintained in such a situation for two hours. Afterward, the ammonia flow is eventually replaced by Ar gas and the temperature of the system is brought to room temperature.[53] Here, the white color BNNTs sample is collected from the boat. The collected sample is characterized for surface morphology, crystallinity, and elemental contents by different characterization instruments.

2.2. Characterization

X-ray diffractometer (XRD) with a CuK radiation (=1.5418) radiation source operating at 40 kV was applied to analyze the

material's structural characteristics. A field emission scanning electron microscope (FESEM) was used to examine the microstructure of the samples (FESEM, Sigma Carl Zeiss). X-ray photoelectron spectra (XPS) were acquired by using a monochromatic AlKa X-ray source (1486.6 eV) on an Omicron GMBH spectrometer. The Raman spectroscopic analysis was carried out by using a RENISHAW spectrometer. The absorption spectra and other photocatalytic measurements were obtained by using an Ultraviolet-visible (Shimadzu UV-2600) spectrophotometer.

2.3. Cytotoxicity assay

The cell lines (HEK-293 (ATCC, CRL-1573) and human cervical cancer (HeLa) (ATCC, CRM-CCL-2)) were purchased from ATCC. These cells were kept in Dulbecco's medium (Is cove's modified) supplemented with penicillin (100 μg mL^{-1}), streptomycin (100 μg mL^{-1}), fetal calf serum (FCS) (10%), and 2 mM Gluta MAX and incubated at 37 °C in an environment of CO_2 (5%) and air (95%) at 90% moisture content for cytotoxicity assays. HeLa (cervical cancer) cell lines were tested for cytotoxicity. 5×10^3 cells per well were incubated in varying concentrations of BNNTs (2 mM L-glutamine, and RPMI-1640 (100 μL) supplemented with 10% FCS). The cytotoxic activity of BN-NTs was investigated in a 96-well microtiter plate by using a standard MTT assay for 24 and 48 hours. MTT is a test (non-radioactive) used to check the vitality of cell cultures regularly. Each well received 20 μL of MTT dye (5 mg mL^{-1} in phosphate-buffered saline) solution quickly after the incubation time. The crystals obtained by the cellular reduction of MTT were dissolved in 120 μL of dimethyl sulfoxide. Using ELISA-reader with a 570 nm filter, plates were read after another 4 hours of incubation. Triplicate's data were collected and the percentage of control wells with cells (without BNNTs) to their relative cell viability was calculated by using the relation:

$$\frac{[A]_{\text{test}}}{[A]_{\text{control}}} \times 100 \quad (1)$$

where $[A]_{\text{control}}$ and $[A]_{\text{test}}$ represent the absorbance of the control and test sample. Researchers were capable to calculate the extent of MTT cleaved, which has a direct relation with the viable cell population, by using a non-radioactive test for cell proliferation.

2.4. Photocatalytic activity

For the removal of MO dye from aqueous solutions, dye degradation studies were performed to investigate the adsorbent characteristics of BNNTs. The dye stock solutions were made by dissolving a precisely measured amount of solid dye in deionized water (DI). Dye solution (100 mL) with a defined quantity was placed in a glass beaker (250 mL) and sonicated to scatter a specific catalyst amount. On a magnetic stirrer, the dispersed solution was consistently stirred at a constant speed of 100 rpm. The solutions were extracted and filtered by using

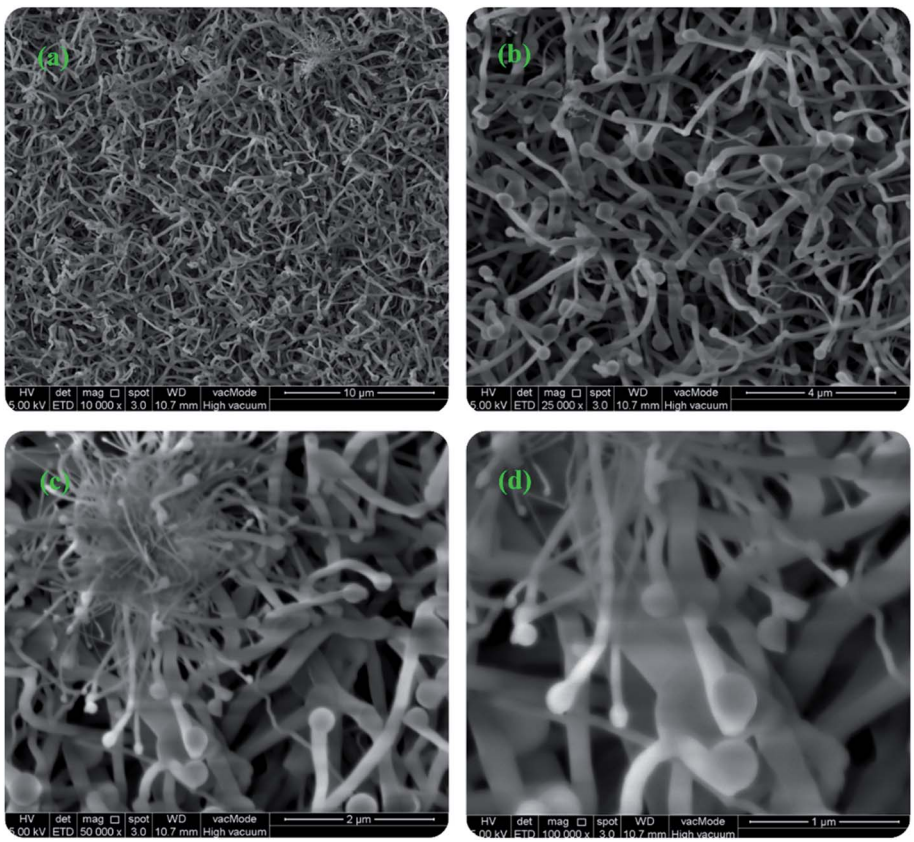

Fig. 1 FESEM micrographs of boron nitride nanotubes with various magnifications (a) 10 000×, (b) 25 000×, (c) 50 000×, and (d) 100 000×.

a nylon syringe filter (0.45 m) to assess the remaining dye concentrations after predefined time intervals. A UV-Vis spectrophotometer tuned to 466 nm was used to measure the preliminary and final concentrations in aqueous solutions. The percentage of dye removal effectiveness by BNNTs was estimated by using the following equation after assessing the UV-Vis data:

$$\text{degradation}\% = \frac{C_0 - C_t}{C_0} \times 100 \quad (2)$$

where degradation% represents the removal percentage of MO dye, C_t represents the concentration of dye (after degradation) at any time, and C_0 is the initial concentration of dye. The effect of experimental conditions on adsorption, such as pH, time, initial dye concentration, and amount of catalyst was thoroughly explored.

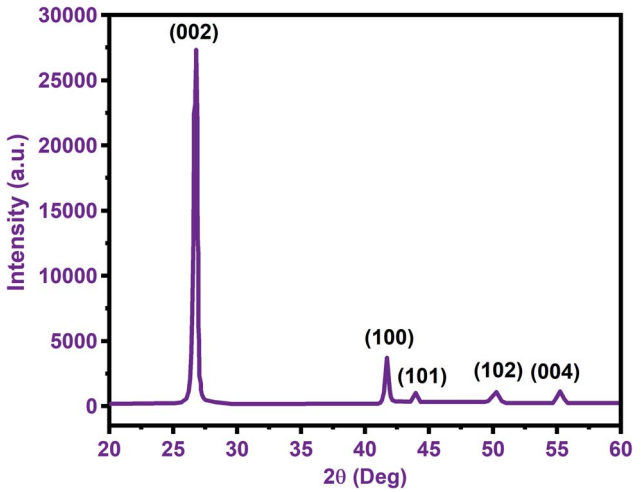

Fig. 2 XRD spectrum of BNNTs shows various peaks corresponding to its highly crystalline nature.

3 Results and discussion

3.1. Field emission scanning electron microscope (FESEM) analysis

The apparent structure, size, and morphology of the as-obtained BNNTs were observed by field emission scanning electron microscopy (FESEM). Morphological characteristics of BNNTs in lower (10 000×, 25 000×) and higher (50 000×, 100 000×) magnification are shown in Fig. 1. The size and morphology of synthesized BNNTs are shown to be greatly influenced by the growth period. The diameter of BNNTs is non-uniform and continuously varies throughout the sample, ranging from 15 to 150 nm, as seen in Fig. 1(a)–(d). The tube's length is likewise variable, ranging from 5 to 10 μm. Some of the

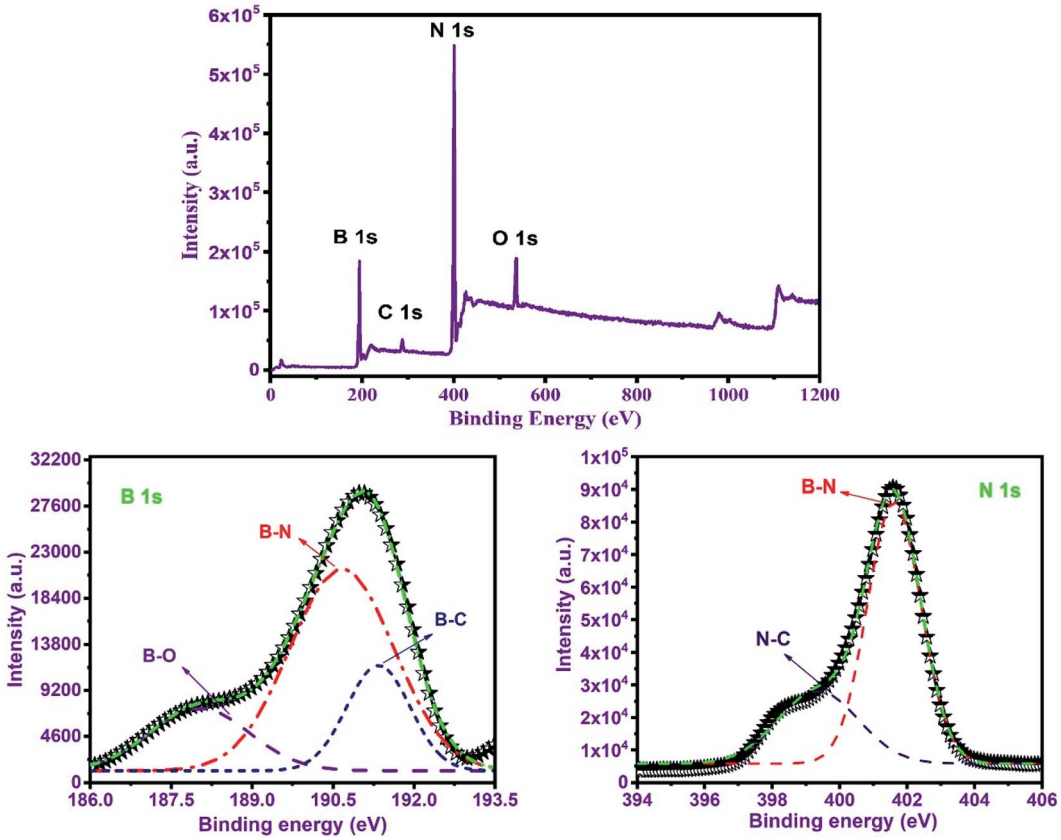

Fig. 3 XPS analysis of the as-synthesized BNNTs. The wide-scanned N 1s and B 1s spectra for nitrogen and boron contents of BNNTs are shown in the bottom left and right-hand corners.

BNNTs are very large whereas some are very small. Overall, the longer tube has a lower diameter than the shorter one, according to the findings. The micrographs show randomly aligned BNNTs with obvious tips at their tops.

3.2. X-ray diffraction (XRD) analysis

The structural properties (elemental composition and phase) of BNNTs were observed by the XRD. The XRD spectrum displayed in Fig. 2 shows a high-intensity peak at 26.8° consistent with the Miller indices of (002). The other peaks in the spectrum at 41.7°, 44.0°, 50.25°, and 55.22° correspond to the Miller indices of (100), (101), (102), and (004) according to the JCPDS no: 034-0421. The sharpness of the peaks shows that all the BNNTs are highly crystalline.[54]

3.3. X-ray photoelectron spectroscopy (XPS) analysis

XPS was used to assess the elemental compositions of the as-prepared BNNTs. B 1s (at 191 eV), C 1s (285 eV), N 1s (at 398.5 eV), and O 1s (533 eV) are the peaks tagged in the survey shown in Fig. 3. The binding energies of B 1s and N 1s peaks correspond to boron and nitrogen concentrations in the as-prepared BNNTs sample with h-BN nature.[55,56] The wide scanned B 1s and N 1s spectra were also obtained to identify the possible impurities in the as-prepared sample shown on the bottom right and left-hand corners of Fig. 3. As can be seen, none of the wide scanned images are degraded. Both, on the other hand, are of Gaussian type.[57] This rule eliminates the possibility of raw materials or precursors appearing as impurities in the prepared material. XPS survey in Fig. 3 also shows the O 1s and C 1s peaks. Both of these peaks could be the result of the material being exposed to the air while being analyzed by XPS.[57]

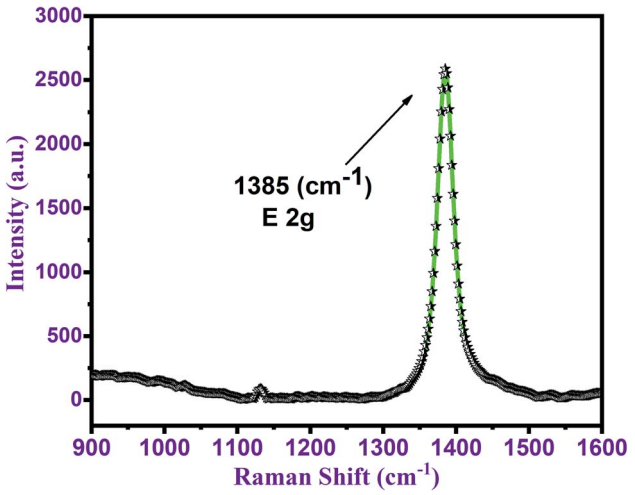

Fig. 4 Raman spectrum with a major peak at 1385 (cm^{-1}) corresponds to the h-BN nature of the synthesized BNNTs.

3.4. Raman spectroscopic analysis

The ^{10}B-contents and h-BN structure of the BNNTs were confirmed by using Raman spectroscopy of the as-prepared sample. Fig. 4 shows the as-obtained Raman spectrum acquired in the spectral region of 800–1600 cm^{-1}. The Raman spectrum displays a high-intensity peak at 1385 cm^{-1}. According to the literature, this peak corresponds to the E_{2g} mode of vibration with ^{10}B-contents in h-BN.[58] Raman spectra are made up of phonons (lattice vibrations) that are highly influenced by the chemical structure of the supporting material as well as the atomic bonds.[59] Due to the lack of effect among inter-layer interactions, monolayer h-BN generates predicted shortening of the B–N bond across a few layers.[60] A lower intensity peak at 1135 cm^{-1} can also be found in the Raman spectra which refers to a small quantity of H_3BO_3. This is due to spontaneous laser contact with moisture in the air and the sample's ^{10}B or $^{10}B_2O_3$.[61]

3.5. Cytotoxicity analysis

For screening viability in multiple samples, MTT assay is extensively used because it is a simple, affordable, and quick procedure. The assay does not distinguish between different types of cell death and is sensitive to variability. The normal cells and cancer cells viability depends on time and dose. HeLa, a cancerous cell line, demonstrated 65% cytotoxicity after 24 hours of treatment at a concentration of 2 mg mL^{-1}, which

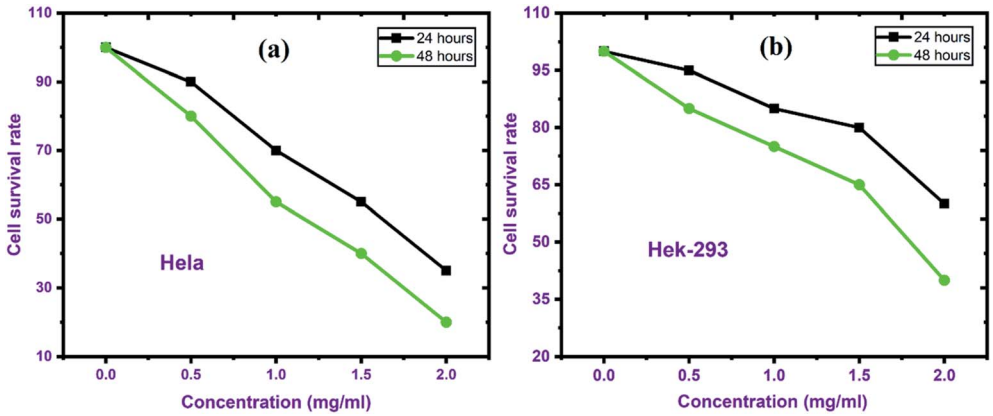

Fig. 5 Cytotoxic effect of BNNTs on HeLa and Hek-293 cell lines, (0.5–2.0 mg mL^{-1}) concentration for 24 & 48 h.

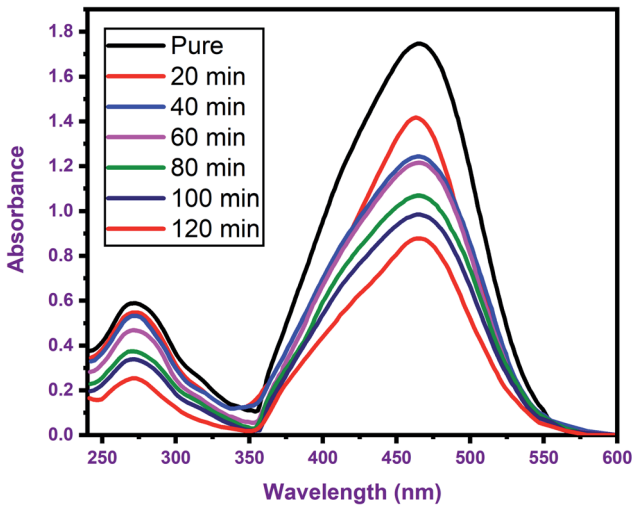

Fig. 6 Absorption spectra of methylene orange dye on BN-NTs surface.

improved up to 80% after 48 hours as shown in Fig. 5(a). In the normal cell line (HEK-293), at 2 mg mL^{-1} dose the cytotoxicity was found 40% and a 24 hour treatment period, increasing to 60% at a later stage (48 hours), as shown in Fig. 5(b). In cancer cells, the cytotoxicity of BNNTs is higher than in normal cell lines. The above results demand further studies to clearly understand the mechanism of cell death.

3.6. Photocatalytic dye-degradation analysis

The degradation of MO dye on the surface of BNNTs was studied to know more about the dye degradation properties of BNNTs. Fig. 6 shows the absorption (UV-Vis) spectra of MO using BNNTs as a catalyst, which exhibits the remarkable degradation properties of BNNTs due to the rapid and intense degradation of the dye on their surface. The impact of several experimental conditions on percent degradation, such as pH, time, initial dye concentration, and catalyst amount, was thoroughly explored.

The degradation efficiency of BNNTs was investigated with varying concentrations for MO dye. The dye concentration was adjusted from 5 to 50 ppm, while the amount of catalyst (0.05 g L^{-1}), pH (4), and contact time (up to 80 minutes) remained constant. When utilizing BNNTs, the percentage of degradation effectiveness was shown to decrease as the starting concentration of dye increased, as shown in Fig. 7(a). This could be due to a decrease in the number of adsorption sites responsible for

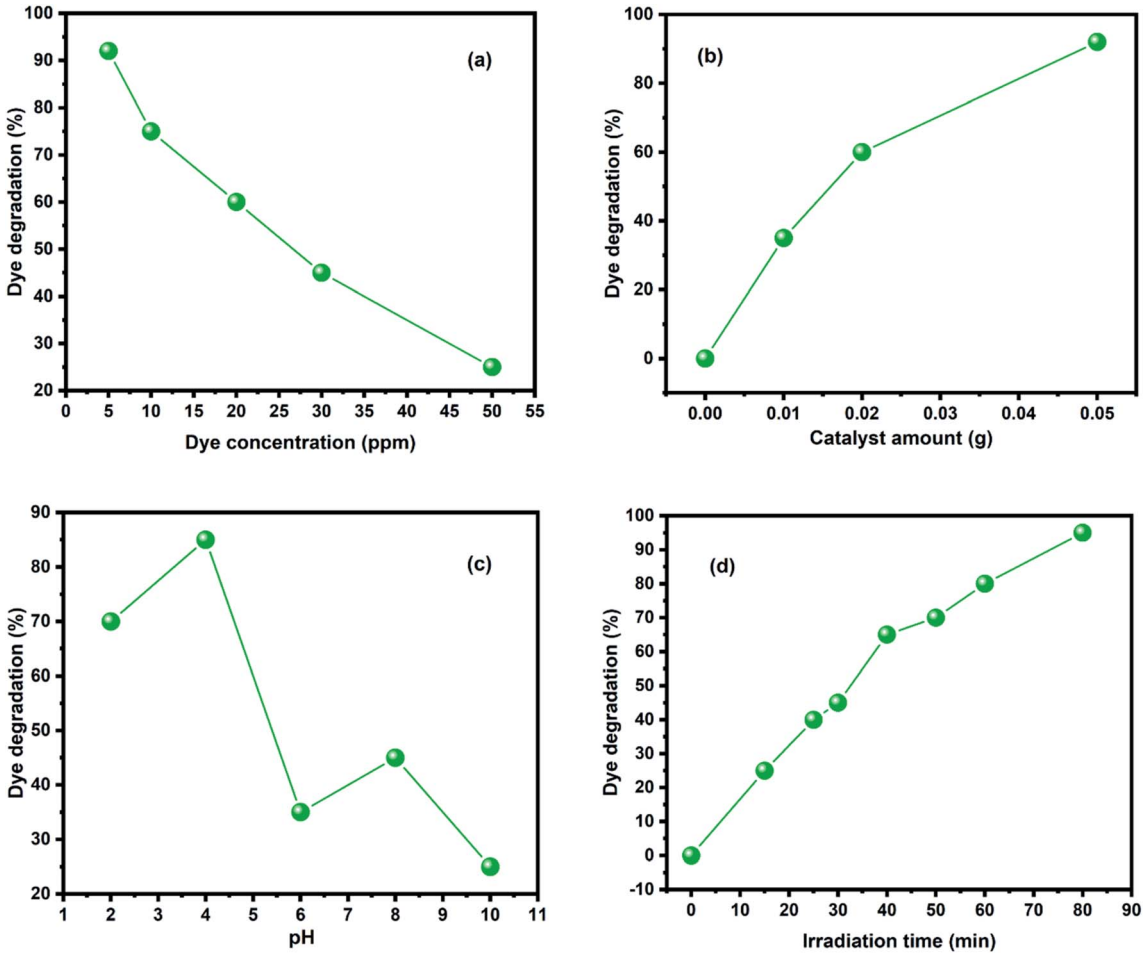

Fig. 7 Photocatalytic dye degradation by BNNTs in terms of (a) initial concentration of dye (5–50 ppm) (b) amount of catalyst (0.01–0.05 g) (c) pH (2–10) and (d) irradiation time (0–80 min).

degradation due to van der Waals interactions b/w catalysts and molecules of dye. A series of adsorption tests were conducted to explore the influence of catalyst amount on the percentage of degradation effectiveness for MO dye. At an initial dye concentration of 0.05 ppm and a pH of solution around 4, the amount of catalyst was adjusted from 0 g L^{-1} to 0.05 g L^{-1} for both dyes. Fig. 7(b) shows the % removal effectiveness of both dyes with various catalyst concentrations of BNNTs. The findings show that, as the amount of catalyst is increased, the percentage degradation efficiency increases, which may be interpreted by enhancement in the adsorption sites available on the catalyst surface. The pH of the solution has a significant impact on dye degradation examinations because it directly affects the surface binding sites, and surface charges of the catalyst as well as the dye molecule's structure. As a result, the influence of pH on % degradation efficiency was investigated by adjusting the solution pH from 2 to 10 using 0.1 M HCl and NaOH solutions, as shown in Fig. 7(c). The degradation efficiency was enhanced at low pH up to 4, possibly resulting in the decline of −ive charge by neutralizing with H^+, however decreased at pH beyond 4, possibly due to increasing competition between H^+ and dye. The presence of a −ive charge on the BNNTs surface is consistent with the outcomes of degradation of dye molecules with different charges at different pH levels, as indicated by the zeta potential. As a result, the degradation of dyes is considered to be extremely specific to the charge present on the catalyst's surface. In degradation studies, time is a critical component in determining the rate of degradation. Lian *et al.*,[43] discovered rapid dye degradation on the surface of BNNSs. In this work, similar adsorption behavior with a high degradation rate was observed, with most degradation occurring in the first 15 minutes and a modest increase is detected after 80 minutes of exposure as shown in Fig. 7(d). As a result, we may classify BNNTs as an ultrafast catalyst that would be extremely valuable for the rapid and considerable destruction of hazardous chemicals.

4 Conclusion

High quality of BNNTs was synthesized in a horizontal quartz tube furnace at 1200 °C and affectively tested for its potential biomedical applications (for their cytotoxic and catalytic potential) to see how they stimulated the normal and cancer cell lines. The viability of normal cells (HEK-293) and cancer cells (HeLa) was assessed by using an MTT assay. The cytotoxicity of BNNTs was explored and found excellent in comparison to previously used materials. It has been found that the cytotoxicity of BNNTs is higher in cancer cells (65 & 80%) than in normal cell lines (40 & 60%) for 24 h and 48 h respectively. The catalytic activity of BNNTs was investigated by observing their performance in the dye degradation process. The degradation behavior of the prepared BNNTs towards the adsorption of methyl orange (MO) dye, is also found very good. Variations in experimental parameters such as initial dye concentration, adsorbent dosage, pH, and time were used to optimize the degradation conditions. The degradation effectiveness decreases (92–25%) as the original concentration of dye increases (5–50 ppm). Similarly, the degradation efficiency improves up to 90% as the amount of catalyst increases from 0.01 g to 0.05 g and the maximum influence of pH was observed at pH 4. Our results show that lower concentrations of BNNTs can be employed in biomedical applications. Dye degradation properties of BNNTs suggest that they can be a potential candidate for wastewater and air treatment materials.

Funding

This work was supported by the Higher Education Commission of Pakistan (HEC) under National Research Program for Universities (NRPU) project no. 10928. The author (Imen Kebaili) also extends its appreciation to the Deanship of Scientific Research at King Khalid University, Saudi Arabia for funding this work through Research Groups Program under grant number R.G.P.1/261/43.

Conflicts of interest

The authors declare no conflict of interest.

Acknowledgements

The authors extend their appreciation to the Higher Education Commission of Pakistan (HEC) for providing funds for our research work under the National Research Program for Universities (NRPU) project no 10928. The author (Imen Kebaili) also extends its appreciation to the Deanship of Scientific Research at King Khalid University, Saudi Arabia for funding this work through Research Groups Program under grant number R.G.P.1/261/43.

References

1 B. N. Singh, *et al.*, Biosynthesis of stable antioxidant ZnO nanoparticles by Pseudomonas aeruginosa rhamnolipids, *PLoS One*, 2014, **9**(9), e106937.
2 A. Rafiq, *et al.*, Photocatalytic and catalytic degradation of organic dye by uncapped and capped ZnS quantum dots, *Mater. Res. Express*, 2019, **6**(5), 055801.
3 M. Ikram, *et al.*, Photocatalytic and bactericidal properties and molecular docking analysis of TiO 2 nanoparticles conjugated with Zr for environmental remediation, *RSC Adv.*, 2020, **10**(50), 30007–30024.
4 A. Raza, *et al.*, Enhanced industrial dye degradation using Co doped in chemically exfoliated MoS2 nanosheets, *Appl. Nanosci.*, 2020, **10**(5), 1535–1544.
5 A. Raza, *et al.*, Liquid-phase exfoliated MoS 2 nanosheets doped with p-type transition metals: a comparative analysis of photocatalytic and antimicrobial potential combined with density functional theory, *Dalton Trans.*, 2021, **50**(19), 6598–6619.
6 C. Allard, *et al.*, Confinement of dyes inside boron nitride nanotubes: photostable and shifted fluorescence down to the near infrared, *Adv. Mater.*, 2020, **32**(29), 2001429.

7 A. Singh, *et al.*, Temperature induced modifications in shapes and crystal phases of MoO3 for enhanced photocatalytic degradation of dye waste water pollutants under UV irradiation, *J. Alloys Compd.*, 2019, **806**, 1368–1376.
8 H. Ouyang, *et al.*, The morphology evolution of nitrogen-doped carbon quantum dots/hollow TiO 2 composites and their applications in photocatalysis, *J. Mater. Sci.*, 2020, **55**(3), 976–989.
9 Z. Razzaq, *et al.*, Photocatalytic and Antibacterial Potency of Titanium Dioxide Nanoparticles: A Cost-Effective and Environmentally Friendly Media for Treatment of Air and Wastewater, *Catalysts*, 2021, **11**(6), 709.
10 U. Qumar, *et al.*, Synergistic effect of Bi-doped exfoliated MoS 2 nanosheets on their bactericidal and dye degradation potential, *Dalton Trans.*, 2020, **49**(16), 5362–5377.
11 M. Zubair, *et al.*, Starch-NiFe-layered double hydroxide composites: efficient removal of methyl orange from aqueous phase, *J. Mol. Liq.*, 2018, **249**, 254–264.
12 I. Ihsanullah, Boron nitride-based materials for water purification: progress and outlook, *Chemosphere*, 2021, **263**, 127970.
13 I. Ihsanullah, M. Bilal and A. Jamal, Recent Developments in the Removal of Dyes from Water by Starch-Based Adsorbents, *Chem. Rec.*, 2022, e202100312.
14 N. Savage and M. S. Diallo, Nanomaterials and water purification: opportunities and challenges, *J. Nanoparticle Res.*, 2005, **7**(4), 331–342.
15 B. B. Sharma and A. Parashar, Mechanical strength of a nanoporous bicrystalline h-BN nanomembrane in a water submerged state, *Phys. Chem. Chem. Phys.*, 2020, **22**(36), 20453–20465.
16 A. Khalid, *et al.*, A practical method for incorporation of Fe (III) in Titania matrix for photocatalytic applications, *Mater. Res. Express*, 2021, **8**(4), 045006.
17 T. Wu, *et al.*, Application of QD-MOF composites for photocatalysis: Energy production and environmental remediation, *Coord. Chem. Rev.*, 2020, **403**, 213097.
18 A. Khalid, *et al.*, Unmodified Titanium Dioxide Nanoparticles as a Potential Contrast Agent in Photon Emission Computed Tomography, *Crystals*, 2021, **11**(2), 171.
19 Y. Huang, *et al.*, Thin-walled boron nitride microtubes exhibiting intense band-edge UV emission at room temperature, *Nanotechnology*, 2009, **20**(8), 085705.
20 M. Ikram, *et al.*, 2D chemically exfoliated hexagonal boron nitride (hBN) nanosheets doped with Ni: synthesis, properties and catalytic application for the treatment of industrial wastewater, *Appl. Nanosci.*, 2020, **10**(9), 3525–3528.
21 Y. N. Xu and W. Ching, Calculation of ground-state and optical properties of boron nitrides in the hexagonal, cubic, and wurtzite structures, *Phys. Rev. B: Condens. Matter Mater. Phys.*, 1991, **44**(15), 7787.
22 X. Chen, *et al.*, Boron nitride nanotubes are noncytotoxic and can be functionalized for interaction with proteins and cells, *J. Am. Chem. Soc.*, 2009, **131**(3), 890–891.
23 A. Salvetti, *et al.*, *In vivo* biocompatibility of boron nitride nanotubes: effects on stem cell biology and tissue regeneration in planarians, *Nanomedicine*, 2015, **10**(12), 1911–1922.
24 X. Li, *et al.*, Hollow boron nitride nanospheres as boron reservoir for prostate cancer treatment, *Nat. Commun.*, 2017, **8**, 13936.
25 A. Khalid, *et al.*, Synergistic effects of Cu-doped ZnO nanoantibiotic against Gram-positive bacterial strains, *PLoS One*, 2021, **16**(5), e0251082.
26 D. Lahiri, *et al.*, Boron nitride nanotube reinforced hydroxyapatite composite: mechanical and tribological performance and *in vitro* biocompatibility to osteoblasts, *J. Mech. Behav. Biomed. Mater.*, 2011, **4**(1), 44–56.
27 L. Liu, *et al.*, Effect of hexagonal boron nitride on high-performance polyether ether ketone composites, *Colloid Polym. Sci.*, 2016, **294**(1), 127–133.
28 L. Horvath, *et al.*, *In vitro* investigation of the cellular toxicity of boron nitride nanotubes, *ACS Nano*, 2011, **5**(5), 3800–3810.
29 A. Khalid, *et al.*, Enhanced Optical and Antibacterial Activity of Hydrothermally Synthesized Cobalt-Doped Zinc Oxide Cylindrical Microcrystals, *Materials*, 2021, **14**(12), 3223.
30 A. Raza, *et al.*, Molecular docking and DFT analyses of magnetic cobalt doped MoS2 and BN nanocomposites for catalytic and antimicrobial explorations, *Surface. Interfac.*, 2021, **27**, 101571.
31 Y. Wang, Z. Shi and J. Yin, Boron nitride nanosheets: large-scale exfoliation in methanesulfonic acid and their composites with polybenzimidazole, *J. Mater. Chem.*, 2011, **21**(30), 11371–11377.
32 M. Ikram, *et al.*, Promising performance of chemically exfoliated Zr-doped MoS 2 nanosheets for catalytic and antibacterial applications, *RSC Adv.*, 2020, **10**(35), 20559–20571.
33 M. Ikram, *et al.*, Hydrothermal synthesis of silver decorated reduced graphene oxide (rGO) nanoflakes with effective photocatalytic activity for wastewater treatment, *Nanoscale Res. Lett.*, 2020, **15**(1), 1–11.
34 M. Ikram, *et al.*, Reduced graphene oxide nanosheets doped by Cu with highly efficient visible light photocatalytic behavior, *J. Alloys Compd.*, 2020, **837**, 155588.
35 C. Tang, *et al.*, Synthetic routes and formation mechanisms of spherical boron nitride nanoparticles, *Adv. Funct. Mater.*, 2008, **18**(22), 3653–3661.
36 M. Ikram, *et al.*, Outstanding performance of silver-decorated MoS2 nanopetals used as nanocatalyst for synthetic dye degradation, *Phys. E*, 2020, **124**, 114246.
37 D. Golberg, *et al.*, Boron nitride nanotubes, *Adv. Mater.*, 2007, **19**(18), 2413–2432.
38 J. Peng, *et al.*, Fabrication of graphene quantum dots and hexagonal boron nitride nanocomposites for fluorescent cell imaging, *J. Biomed. Nanotechnol.*, 2013, **9**(10), 1679–1685.
39 J. Li, *et al.*, Constructing h-BN/Bi2WO6 Quantum Dot Hybrid with Fast Charge Separation and Enhanced Photoelectrochemical Performance by using h-BN for Hole Transfer, *ChemElectroChem*, 2018, **5**(2), 300–308.

40 M. Nasr, *et al.*, High photodegradation and antibacterial activity of BN–Ag/TiO 2 composite nanofibers under visible light, *New J. Chem.*, 2018, **42**(2), 1250–1259.
41 V. Štengl, J. Henych and M. Slušná, h-BN-TiO2 nanocomposite for photocatalytic applications, *J. Nanomater.*, 2016, 4580516.
42 X. Zhang, *et al.*, Boron nitride nanocarpets: controllable synthesis and their adsorption performance to organic pollutants, *CrystEngComm*, 2012, **14**(14), 4670–4676.
43 G. Lian, *et al.*, Boron nitride ultrathin fibrous nanonets: one-step synthesis and applications for ultrafast adsorption for water treatment and selective filtration of nanoparticles, *ACS Appl. Mater. Interfaces*, 2013, **5**(24), 12773–12778.
44 T. Terao, *et al.*, Effective synthesis of surface-modified boron nitride nanotubes and related nanostructures and their hydrogen uptake, *Phys. E*, 2008, **40**(7), 2551–2555.
45 R. Chen, *et al.*, Arsenic (V) adsorption on Fe3O4 nanoparticle-coated boron nitride nanotubes, *J. Colloid Interface Sci.*, 2011, **359**(1), 261–268.
46 J. Qu, *et al.*, Characterization of flake boron nitride prepared from the low temperature combustion synthesized precursor and its application for dye adsorption, *Coatings*, 2018, **8**(6), 214.
47 A. Khalid, *et al.*, Structural, Optical and Antibacterial Efficacy of Pure and Zinc-Doped Copper Oxide against Pathogenic Bacteria, *Nanomaterials*, 2021, **11**(2), 451.
48 F. Liu, *et al.*, Nanosheet-structured boron nitride spheres with a versatile adsorption capacity for water cleaning, *ACS Appl. Mater. Interfaces*, 2015, **7**(3), 1824–1832.
49 J. Li, *et al.*, Chemical activation of boron nitride fibers for improved cationic dye removal performance, *J. Mater. Chem. A*, 2015, **3**(15), 8185–8193.
50 J. Li, *et al.*, Activated boron nitride as an effective adsorbent for metal ions and organic pollutants, *Sci. Rep.*, 2013, **3**(1), 1–7.
51 Q. Li, *et al.*, Porous hexagonal boron nitride whiskers fabricated at low temperature for effective removal of organic pollutants from water, *Ceram. Int.*, 2016, **42**(7), 8754–8762.
52 M. Ikram, *et al.*, Dye degradation performance, bactericidal behavior and molecular docking analysis of Cu-doped TiO 2 nanoparticles, *RSC Adv.*, 2020, **10**(41), 24215–24233.
53 P. Ahmad, *et al.*, The antibacterial and antioxidant efficacy and neutron sensing potency of 10B enriched hexagonal boron nitride nanoparticles, *Mater. Sci. Semicond. Process.*, 2022, **141**, 106419.
54 R. Kasar, *et al.*, Studies and correlation among the structural, optical and electrical parameters of spray-deposited tin oxide (SnO2) thin films with different substrate temperatures, *Phys. B*, 2008, **403**(19–20), 3724–3729.
55 S. Sinnott, *et al.*, Model of carbon nanotube growth through chemical vapor deposition, *Chem. Phys. Lett.*, 1999, **315**(1), 25–30.
56 C.-Y. Su, *et al.*, Large-scale synthesis of boron nitride nanotubes with iron-supported catalysts, *J. Phys. Chem. C*, 2009, **113**(33), 14732–14738.
57 B. Zhong, *et al.*, Synthesis of boron nitride nanotubes with SiC nanowire as template, *Mater. Res. Bull.*, 2011, **46**(9), 1521–1523.
58 W. Q. Han, *et al.*, Isotope effect on band gap and radiative transitions properties of boron nitride nanotubes, *Nano Lett.*, 2008, **8**(2), 491–494.
59 B. Singh, *et al.*, Nanostructured boron nitride with high water dispersibility for boron neutron capture therapy, *Sci. Rep.*, 2016, **6**(1), 1–10.
60 D. Lee and S. H. Song, Ultra-thin ultraviolet cathodoluminescent device based on exfoliated hexagonal boron nitride, *RSC Adv.*, 2017, **7**(13), 7831–7835.
61 R. Arenal, *et al.*, Raman spectroscopy of single-wall boron nitride nanotubes, *Nano Lett.*, 2006, **6**(8), 1812–1816.